Anomalous diffusion in branched elliptical structure

Kheder Suleiman[1,2], Xuelan Zhang(张雪岚)[2], Erhui Wang(王二辉)[1], Shengna Liu(刘圣娜)[1], and Liancun Zheng(郑连存)[2,†]

[1] *School of Energy and Environmental Engineering, University of Science and Technology Beijing, Beijing* 100083, *China*
[2] *School of Mathematics and Physics, University of Science and Technology Beijing, Beijing* 100083, *China*

(Received 16 January 2022; revised manuscript received 1 March 2022; accepted manuscript online 10 March 2022)

Diffusion in narrow curved channels with dead-ends as in extracellular space in the biological tissues, e.g., brain, tumors, muscles, etc. is a geometrically induced complex diffusion and is relevant to different kinds of biological, physical, and chemical systems. In this paper, we study the effects of geometry and confinement on the diffusion process in an elliptical comb-like structure and analyze its statistical properties. The ellipse domain whose boundary has the polar equation $\rho(\theta) = \frac{b}{\sqrt{1-e^2\cos^2\theta}}$ with $0 < e < 1$, $\theta \in [0, 2\pi]$, and b as a constant, can be obtained through stretched radius r such that $\Upsilon = r\rho(\theta)$ with $r \in [0,1]$. We suppose that, for fixed radius $r = R$, an elliptical motion takes place and is interspersed with a radial motion inward and outward of the ellipse. The probability distribution function (PDF) in the structure and the marginal PDF and mean square displacement (MSD) along the backbone are obtained numerically. The results show that a transient sub-diffusion behavior dominates the process for a time followed by a saturating state. The sub-diffusion regime and saturation threshold are affected by the length of the elliptical channel lateral branch and its curvature.

Keywords: anomalous diffusion, Fokker–Planck equation, branched elliptical structure

PACS: 02.50.Fz, 02.50.Ey, 05.40.–a, 05.60.–k **DOI:** 10.1088/1674-1056/ac5c39

1. Introduction

Diffusion is an essential means of transportation in biological, physical, and chemical systems that is used by individuals to achieve their functions, for example, but not limited to, cellular processes, metabolism, and conduction.[1–5] Realizing the features of diffusion, which depend on its microscopic dynamics and environmental space, will provide an important tool to control these processes, besides its possible applications in nanotechnology and nanomedicine. According to the theory of Brownian motion, the probability distribution is Gaussian and mean square displacement (MSD) of the particle position grows linearly with time $\langle r^2(t)\rangle = 2Dt$ where D is the diffusion coefficient. However, deviations from these usual behaviors have been observed theoretically and experimentally, anomalous (non-Brownian) diffusion,[6–10] Brownian yet non-Gaussian diffusion,[11–13] and anomalous yet non-Gaussian diffusion.[14,15] The nonlinear dependence of time characterizes the MSD in the anomalous dynamics, namely, $\langle r^2(t)\rangle] \sim t^{\alpha}$ with $\alpha \neq 1$. The diffusion dynamics with transport exponent $0 < \alpha < 1$ correspond to sub-diffusion dynamics which are observed in artificially crowded liquids,[16] lipid bilayer membranes,[15,17] the cytoplasm of biological cells,[18] extracellular space,[19] and in hydrology,[20] to mention a few. Whereas, it defines super-diffusion when $\alpha > 1$, which is encountered in active systems such as molecular motor transport in cells.[21,22] Different hypotheses have been suggested to understand the mechanism underlying sub-diffusion dynamics, which depends on the situation at hand, among them, trapping models of energetic (binding sites) or geometric nature, labyrinthine environment (geometrical disorder), temporal correlation due to slow mode (viscoelastic environments), space-dependent diffusivity due to the local porosity of the medium or temperature field in the sense of weak gradients, which can be modelled by continuous time random walk (CTRW), random walk on fractals, fractional Brownian motion (FBM) or fractional Langevin equation (FLE), and heterogeneous diffusion process (HDP), respectively.[8,23–27]

Disordered materials in nature are abundant, including to mention a few the heterogeneous porous media, extracellular space in brain tissue, intra-tissue in muscles, cell cytoplasm, and glasses.[28–35] Diffusion in disordered media is quite affected by its geometrical structure, for instance, dead ends, bottlenecks, and backends. Since deterministic fractals and percolation clusters are elegant models for the geometrical structure of disorder systems, Pierre-Gilles de Gennes has suggested modelling diffusion in these systems through performing random walks on percolation clusters and fractals, and coined the term "ant in the labyrinth".[26] Random walks in these structures lead to anomalous diffusion. At the percolation threshold, a percolation structure can be idealized as a single infinite cluster, consisting of a conducting path, which corresponds to a backbone, and side branches, or fingers with dangling bonds. At some level of idealization, this structure corresponds to a comb.[36] Later, the comb-like structure consisting of the one-dimensional axis (backbone) with perpendicular sides branches (fingers) has been used to understand

†Corresponding author. E-mail: liancunzheng@ustb.edu.cn

© 2023 Chinese Physical Society and IOP Publishing Ltd

the underlying mechanism of anomalous diffusion in percolation clusters: while the particle moving randomly along the backbone may trap inside the dead-ends (fingers), performing a Brownian motion, until it returns by chance to the backbone where it can escape from the finger. Along the y-direction (the so-called fingers), the particles perform normal diffusion, while the mean square displacement (MSD) along the backbone grows non-linearly with a time $\langle x^2(t)\rangle \simeq \sqrt{t}$, and sub-diffusion behavior dominates the process.[26,37,38]

To study the transport properties of diffusion process on comb-like structure, different approaches have been applied, e.g., a mesoscopic approach used by Weiss and Havlin,[37] a macroscopic approach used by Arkhincheev and Baskin,[39] and a microscopic approach used by Méndez *et al.*[40] Arkhincheev and Baskin have expressed the diffusion process in the comb by using the following Fokker–Planck equation:[39]

$$\frac{\partial P(x,y,t)}{\partial t} = \delta(y)\tilde{D}\frac{\partial^2 P(x,y,t)}{\partial x^2} + D\frac{\partial^2 P(x,y,t)}{\partial y^2}.$$

Here, $D_x = \delta(y)\tilde{D}$ and $D_y = D$ are the diffusion coefficients in the x and y directions, respectively, and the δ-function in the Fokker–Planck operator $L_{\rm FP} = \delta(y)\tilde{D}\frac{\partial^2}{\partial x^2} + D\frac{\partial^2}{\partial y^2}$ means that the diffusion along the x direction (the so called backbone) is allowed only at $y = 0$.

Recently, comb-like model has been used to describe anomalous diffusion in spiny dendrites,[41] the mechanism of super-diffusion of ultracold atoms in a one-dimensional as a phenomenology of experimental study,[42] as well as anomalous diffusion in porous materials.[43] Moreover, several complex extensions of comb-like structure, through introducing a modification on the geometry of the backbone or finger shape of the structure, is introduced to describe geometrically induced complex diffusion in nature, for example, comb with a finite finger length,[40,44,45] cylindrical comb,[46,47] random comb models,[48,49] comb with ramified teeth,[40,41] fractal mesh and grid structures,[50–52] and more complex structure.[53–57] Diffusion along the backbone in both two and three-dimensional comb-like structures with a finite finger is a transient sub-diffusion followed by normal diffusion at long times, and the same result is obtained in using a trap model of energetic nature.[58] Whereas, diffusion along the backbone in a three-dimensional comb-like structure with an infinite two-dimensional branch is ultra-slow diffusion/enhanced sub-diffusion if normal/sub-diffusion occurs inside branches.[46,47] In addition, recent theoretical studies have been demonstrating that performing different microscopic dynamics in a comb-like model leads to different types of anomalous diffusion.[59–63] In most previous studies, the geometric properties of the backbone have not been considered. However, the interior of disordered systems are narrow, tortuous, curved channels.[26,64,65]

In the last decade, the problem of diffusion in curved confined tubes has attracted remarkable attention of some researchers, as it was found that the behavior of the diffusion process is affected by its geometrical properties, like curvature and torsion, of these tubes.[66–69] This problem is related to diverse kinds of phenomena, for example not limited to, diffusion of biomolecules in biological cell,[70] transport of solute in aquifers and porous medium, and fluxon dynamics in Josephson junction.[71] The aim of this paper is to study the diffusive dynamics in branched channels with gradient curvature. Branched elliptical-like channels are common in biology, including to mention a few, the extracellular spaces in the biological tissues (brain, tumors, muscles), intracellular environments, and other porous media,[19,31,72–78] in which diffusion process in these structures are important for other biological processes like extracellular ionic buffering, and delivery of drugs and metabolites, etc.[79,80] Moreover, they are simple models of curved confined sub-diffusive systems with gradient curvature. Motivated by the foregoing, we analyze the dynamics of the diffusion process in an elliptical comb-like structure (see Fig. 1) with reflected boundary conditions. The elliptical motion takes place only for a fixed radius $r = R$ and is interspersed with a radial motion inward and outward of the ellipse. The Brownian radial motion corresponds to diffusion of particles in dead-end spaces, while elliptical backbone describes the dynamics along elliptical channels. We investigate by numerical simulation how probability distribution function (PDF) and mean square displacement (MSD) are affected by geometrical constraints in the elliptical comb-like structure.

The rest of the paper is organized as follows. We firstly formulate the mathematical description of the problem in Section 2. The numerical method and example on the verification of the numerical algorithm are collected in Section 3. Then results and discussion are illustrated in Section 4. The conclusions are given in Section 5.

2. Mathematical formulation

The structure we study here consists of elliptical channel with radii dead ends distributed along it and directed in/outside (see Fig. 1), in which an unbiased diffusion process occurs inside it. Mathematically, suppose an ellipse whose boundary has the polar equation $\rho(\theta) = b/\sqrt{1-e^2\cos^2\theta}$, where $0 < e < 1$ is the eccentricity of ellipse, b is the shortest diameter with constant value, and $\theta \in [0, 2\pi]$. Then, its domain can be obtained through stretched radius r such that $\Upsilon = r\rho(\theta)$ with $\theta \in [0, 2\pi]$, and $r \in [0, 1]$, where we can move from Cartesian coordinates to stretched polar coordinates through the transformation[81]

$$x = r\rho(\theta)\cos\theta, \quad y = r\rho(\theta)\sin\theta. \tag{1}$$

The distinctive feature of diffusion process in such structure is that the particle motion along θ direction is possible only when $r = R$ and R is a constant. We mean that the tangent diffusion coefficient D_θ is different from zero only at $r = R$, i.e., $D_\theta = \tilde{D}\delta(r-R)$ with $\tilde{D}$ is a constant. Whereas, the diffusion is free in the radial direction situation and its diffusion coefficient can be written as $D_r = D$. By adjusting the parameter e the elliptical channel (backbone) has different shapes, in which the curvature of the ellipse , $\kappa = ab/\left(\sqrt{a^2\sin^2\theta + b^2\cos^2\theta}\right)^3$ with $a^2 = b^2/\left(1-e^2\right)$, decreases as the value of e increases (see Fig. 1). In order to assess how particles diffuse in the structure probability distribution function (PDF) $P(r,\theta,t)$, marginal PDF $P(r,t)$, and mean square displacement (MSD) along θ are a useful quantities. In the classical comb model, PDF $P(r,\theta,t)$ can be described by Fokker–Planck equation[39] $\partial_t P = \delta(y)\tilde{D}\partial_x^2 P + D\partial_y^2 P$. The δ function in the Fokker–Planck operator $L_{\rm FP} = \delta(y)\tilde{D}\partial_x^2 + D\partial_y^2$ means that the diffusion along the x direction is allowed only at $y = 0$. In what follows, we derive the diffusion equation in a stretched polar coordinate system, then find the differential equation that expresses the diffusion process in our structure.

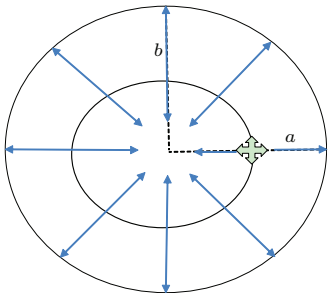


Fig. 1. Schematic picture of an elliptical comb-like structure, where the radii are continuously distributed over the ellipse of radius $R = \rho(\theta)$ with $\theta \in [0, 2\pi]$.

2.1. Derivation of diffusion equation in stretched polar coordinates

The gradient operator can be written as follows:

$$\nabla = \hat{u}_r\left(\frac{1}{\rho(\theta)}\frac{\partial}{\partial r}\right) + \hat{u}_\theta\left(-\frac{\rho'(\theta)}{\rho^2(\theta)}\frac{\partial}{\partial r} + \frac{1}{r\rho(\theta)}\frac{\partial}{\partial\theta}\right). \quad (2)$$

Then, the balance equation and the first Fick's law can be written respectively as follows:

$$\begin{aligned}\frac{\partial P}{\partial t} &= -\nabla\cdot J\\ &= -\left[\frac{1}{\rho(\theta)}\frac{\partial J_r}{\partial r} + \frac{J_r}{r\rho(\theta)}\right.\\ &\quad \left. - \frac{\rho'(\theta)}{\rho^2(\theta)}\frac{\partial J_\theta}{\partial r} + \frac{1}{r\rho(\theta)}\frac{\partial J_\theta}{\partial\theta}\right], \quad (3)\\ J &= -D\nabla P\\ &= -\left[\hat{u}_r\left(\frac{D_r}{\rho(\theta)}\frac{\partial P}{\partial r}\right)\right.\\ &\quad \left. + \hat{u}_\theta\left(-\frac{D_\theta\rho'(\theta)}{\rho^2(\theta)}\frac{\partial P}{\partial r} + \frac{D_\theta}{r\rho(\theta)}\frac{\partial P}{\partial\theta}\right)\right]. \quad (4)\end{aligned}$$

Then the second Fick's equation reads

$$\begin{aligned}\frac{\partial P}{\partial t} &= \frac{1}{\rho^2(\theta)}\left(D_r + \frac{D_\theta\rho'^2(\theta)}{\rho^2(\theta)}\right)\frac{\partial^2 P}{\partial r^2}\\ &\quad + \frac{1}{r\rho^2(\theta)}\left(D_r - \frac{D_\theta\rho''(\theta)}{\rho(\theta)} + \frac{2D_\theta\rho'^2(\theta)}{\rho^2(\theta)}\right)\frac{\partial P}{\partial r}\\ &\quad - 2\frac{D_\theta\rho'(\theta)}{r\rho^3(\theta)}\frac{\partial^2 P}{\partial r\partial\theta} + \frac{D_\theta}{r^2\rho^2(\theta)}\frac{\partial^2 P}{\partial\theta^2}. \quad (5)\end{aligned}$$

2.2. Diffusion equation in elliptical comb-like structure

The dynamic in the structure can be described by the following diffusion equation (substitute $\rho(\theta) = \frac{b}{\sqrt{1-e^2\cos^2\theta}}$, $D_r = D$, and $D_\theta = \tilde{D}\delta(r-R)$ into Eq. (5)):

$$\begin{aligned}\frac{\partial P}{\partial t} &= D\left[\left(\frac{1-e^2\cos^2\theta}{b^2}\right)\frac{\partial^2 P}{\partial r^2} + \left(\frac{1-e^2\cos^2\theta}{b^2 r}\right)\frac{\partial P}{\partial r}\right]\\ &\quad + \tilde{D}\left[\left(\frac{4e^2\cos 2\theta(1-e^2\cos^2\theta) - e^4\sin^2 2\theta}{4b^2 r(1-e^2\cos^2\theta)}\right)\frac{\partial P}{\partial r}\right.\\ &\quad + \left(\frac{e^4\sin^2 2\theta}{4b^2(1-e^2\cos^2\theta)}\right)\frac{\partial^2 P}{\partial r^2}\\ &\quad \left. + \left(\frac{e^2\sin 2\theta}{b^2 r}\right)\frac{\partial^2 P}{\partial r\partial\theta} + \left(\frac{1-e^2\cos^2\theta}{b^2 r^2}\right)\frac{\partial^2 P}{\partial\theta^2}\right]\\ &\quad \times\delta(r-R), \quad (6)\end{aligned}$$

with initial condition

$$P(r,\theta,0) = \delta(r-R)\delta(\theta), \quad (7)$$

and boundary conditions

$$\begin{aligned}\frac{\partial}{\partial\theta}P(R,+\pi,t) &= \frac{\partial}{\partial\theta}P(R,-\pi,t) = 0,\\ \frac{\partial}{\partial r}P(L,\theta,t) &= \frac{\partial}{\partial r}P(R',\theta,t) = 0. \quad (8)\end{aligned}$$

3. Numerical procedure

3.1. Numerical algorithm

The initial–boundary value problem (6)–(8) can be solved numerically by using the following procedure: Firstly, in order to divide the spatial and temporal domain into grid, we define $r_i = ih_r$, $\theta_j = jh_\theta$, and $t_l = l\tau$ where $i = \overline{1, N_r+1}$, $j = \overline{1, N_\theta+1}$, and $l = \overline{1, N_T+1}$, besides $h_r = R'/N_r$, and $h_\theta = \pi/N_\theta$ are space steps, $\tau = T/N_T$ is time step. Let $P_{i,j}^l$ be the numerical solution of Eq.(6) at point (r_i,θ_j,t_l), then the first and second order derivatives in the governing equation can be discretized as follows:

$$\begin{aligned}\partial_t P(r_i,\theta_j,t_l) &= \left(P_{i,j}^{l+1} - P_{i,j}^l\right)/\tau,\\ \partial_r P(r_i,\theta_j,t_l) &= \left(P_{i+1,j}^l - P_{i,j}^l\right)/h_r,\\ \partial_\theta P(r_i,\theta_j,t_l) &= \left(P_{i,j+1}^l - P_{i,j}^l\right)/h_\theta,\\ \partial_\theta^2 P(r_i,\theta_j,t_l) &= \left(P_{i,j+1}^l - 2P_{i,j}^l + P_{i,j-1}^l\right)/h_\theta^2,\\ \partial_r^2 P(r_i,\theta_j,t_l) &= \left(P_{i+1,j}^l - 2P_{i,j}^l + P_{i-1,j}^l\right)/h_r^2,\end{aligned}$$

$$\partial^2_{r\theta}P(r_i,\theta_j,t_l)=\left(P^l_{i+1,j+1}-P^l_{i+1,j}-P^l_{i,j+1}+P^l_{i,j}\right)/h_rh_\theta.$$

Now, applying the previous approximate scheme to Eq. (6) yields the following iterative equations:

$$\begin{aligned}P^{l+1}_{i,j} &= [\lambda^1_j+\lambda^3_{i,j}+(\lambda^2_j+\lambda^4_{i,j}-\lambda^5_{i,j})\delta(r_i-R)]\\ &\times P^l_{i+1,j}+[\lambda^1_j+\lambda^2_j\delta(r_i-R)P^l_{i-1,j}\\ &+[1-2\lambda^1_j-\lambda^3_{i,j}-(2\lambda^2_j+\lambda^4_{i,j}-\lambda^5_{i,j}+2\lambda^6_{i,j})\\ &\times\delta(r_i-R)]P^l_{i,j}+[(\lambda^6_{i,j}-\lambda^5_{i,j})\delta(r_i-R)]P^l_{i,j+1}\\ &+[\lambda^6_{i,j}\delta(r_i-R)]P^l_{i,j-1}+[\lambda^5_{i,j}\delta(r_i-R)]P^l_{i+1,j+1},\end{aligned}\tag{9}$$

where

$$\begin{aligned}\lambda^1_j &= \frac{D(1-e^2\cos^2\theta_j)\tau}{b^2h_r^2},\\ \lambda^2_j &= \frac{\tilde{D}e^4\sin^2(2\theta_j)\tau}{4b^2h_r^2(1-e^2\cos^2\theta_j)},\\ \lambda^3_{i,j} &= \frac{D(1-e^2\cos^2\theta_j)\tau}{b^2r_ih_r},\\ \lambda^4_{i,j} &= \frac{4\tilde{D}e^2\cos2\theta_j(1-e^2\cos^2\theta_j)\tau-\tilde{D}e^4\sin^2(2\theta_j)\tau}{4b^2r_ih_r(1-e^2\cos^2\theta_j)},\\ \lambda^5_{i,j} &= \frac{\tilde{D}e^2\sin^2(2\theta_j)\tau}{r_ib^2h_rh_\theta},\quad \lambda^6_{i,j}=\frac{\tilde{D}(1-e^2\cos^2\theta_j)\tau}{b^2r_i^2h_\theta^2}.\end{aligned}\tag{10}$$

3.2. Verification of the validity of the numerical solution

In order to test the correctness of numerical solution, we introduce a source function $f(r,\theta,t)$ in Eq. (6), and this yields the following equation:

$$\begin{aligned}\frac{\partial P}{\partial t} &= D\left[\left(\frac{1-e^2\cos^2\theta}{b^2}\right)\frac{\partial^2P}{\partial r^2}+\left(\frac{1-e^2\cos^2\theta}{b^2r}\right)\frac{\partial P}{\partial r}\right]\\ &+\tilde{D}\left[\left(\frac{4e^2\cos2\theta(1-e^2\cos^2\theta)-e^4\sin^22\theta}{4b^2r(1-e^2\cos^2\theta)}\right)\frac{\partial P}{\partial r}\right.\\ &+\left(\frac{e^4\sin^22\theta}{4b^2(1-e^2\cos^2\theta)}\right)\frac{\partial^2P}{\partial r^2}\\ &\left.+\left(\frac{e^2\sin2\theta}{b^2r}\right)\frac{\partial^2P}{\partial r\partial\theta}+\left(\frac{1-e^2\cos^2\theta}{b^2r^2}\right)\frac{\partial^2P}{\partial\theta^2}\right]\\ &\times\delta(r-R)+f(r,\theta,t),\end{aligned}\tag{11}$$

with initial condition

$$P(r,\theta,0)=(r-1)^2(r-L)^2(\theta+\pi)^2(\theta-\pi)^2,\tag{12}$$

and boundary conditions

$$\begin{aligned}\frac{\partial}{\partial r}P(L,\theta,t)=\frac{\partial}{\partial r}P(1,\theta,t)=0,\\ \frac{\partial}{\partial\theta}P(r,-\pi,t)=\frac{\partial}{\partial\theta}P(r,\pi,t)=0,\end{aligned}\tag{13}$$

where

$$\begin{aligned}f(r,\theta,t) &= (r-1)^2(r-L)^2(\theta+\pi)^2(\theta-\pi)^2\\ &-2A(t+1)(r-1)(r-L)\\ &\times(2r-1-L)(\theta+\pi)^2(\theta-\pi)^2\\ &-8B(t+1)(r-1)(r-L)\\ &\times(2r-1-L)(\theta+\pi)(\theta-\pi)\\ &-C(t+1)(12r^2-12rL-12r'\\ &+8L+2L^2+2)(\theta+\pi)^2(\theta-\pi)^2\\ &-4E(t+1)(r-1)^2(r-L)^2(3\theta^2-\pi^2),\end{aligned}$$

with

$$\begin{aligned}A &= \frac{D(1-e^2\cos^2\theta)}{b^2r}\\ &+\frac{\tilde{D}\left[4e^2\cos2\theta(1-e^2\cos^2\theta)-e^4\sin^2(2\theta)\right]\delta(r-R)}{4b^2r(1-e^2\cos^2\theta)},\\ B &= \frac{\tilde{D}e^2\sin^2(2\theta)\delta(r-R)}{rb^2},\\ C &= \frac{D(1-e^2\cos^2\theta)}{b^2}+\frac{\tilde{D}e^4\sin^2(2\theta)\delta(r-R)}{4b^2(1-e^2\cos^2\theta)},\\ E &= \frac{\tilde{D}(1-e^2\cos^2\theta)\delta(r-R)}{b^2r^2}.\end{aligned}$$

The exact solution of the equation is given by

$$P(r,\theta,t)=(t+1)(r-1)^2(r-L)^2(\theta+\pi)^2(\theta-\pi)^2.\tag{14}$$

The comparison between the exact and numerical solution of Eq. (13) subject to the initial condition and boundary conditions Eqs. (12)–(15) is shown in Fig. 2. We can see that the curves in a good agreement which indicates the correctness of numerical results.

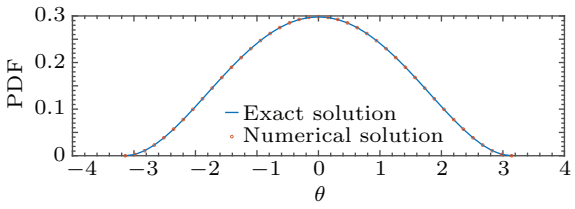


Fig. 2. The comparison of the exact solution via Eq.(16) with numerical solution for $b=1$, $e=0.5$, $D=\tilde{D}=1$, $\tau=10^{-4}$, $h_r=10^{-2}$, and $h_\theta=\pi/20$ at $T=1$.

4. Results and discussion

4.1. Probability distribution function

The probability distribution function (PDF) $P(x,y,t)$ is a useful quantity to assess how particles are distributed in the structure. In case of classical comb with a reflected boundary conditions, the evolution of PDF $P(x,y,t)$ can be described by the comb equation $\partial_tP(x,y,t)=\delta(y-y_0)\tilde{D}\partial^2_xP(x,y,t)+D\partial^2_yP(x,y,t)$ with the following initial and boundary conditions:

$$\begin{aligned}P(x,y,0)=\delta(x-x_0)\delta(y-y_0),\\ \left.\frac{\partial P(x,y_0,t)}{\partial x}\right|_{x\to\pm L}=0,\quad \left.\frac{\partial P(x,y,t)}{\partial y}\right|_{y\to\pm R}=0.\end{aligned}$$

The temporal evolution of marginal PDF $P_1(x,t)=\int_{-R}^{R}P(x,y,t)\,\mathrm{d}y$, which characterizes the distribution of particle along the backbone, is detailed in Figs. 3 and 4. Figure 3

shows that, for fixed L, $P_1(x,t)$ converges to the same non-Gaussian function $\tilde{P}_1(x,t)$ as time increases, and the speed of convergence is inversely proportional to R (the length of the lateral finger $2R$). Moreover, the function $\tilde{P}_1(x,t)$ is affected by L, in which the concentration reduces as the length of the backbone increases, seen in Fig. 4. This means that the particles diffuse slowly, then they saturate after a period due to limited of the backbone. Moreover, the stay time in the branch until they return to the backbone determines the nature of its diffusion and reaches a saturated state. This will be demonstrated in the next subsection. Now, we show the effects of the parameters b and e on the distribution of particles $P(r,\theta,t)$ in the whole elliptical comb-like structure, and the marginal PDF $\widetilde{P}_1(\theta,t)$ along θ direction of the structure. The temporal evolution of the distribution in the structure is drawn from the iterative Eq. (9) by using Matlab. The parameters b and e reflect the geometric properties of the ellipse. The relationship among the shortest diameter b, the longest diameter a, and the eccentricity of ellipse e reads as $a^2 = b^2/(1-e^2)$ with $0 \le e < 1$. Moreover, the curvature of an ellipse is given as $\kappa = ab/\left(\sqrt{a^2\sin^2\theta + b^2\cos^2\theta}\right)^3$. For fixed b, the curvature of the ellipse decreases as the value of e increases. Figure 5 depicts the distribution of particles in the structure with different parameter effects at $T = 1$. It shows that the concentration at the initial position increases as the shortest diameter b and the eccentricity e of ellipse increases. Namely, the diffusion of particles slows down as the length of lateral branches and the curvature of the elliptical channel increase, in which these increments affect the waiting time and obstruction in the diffusion process.

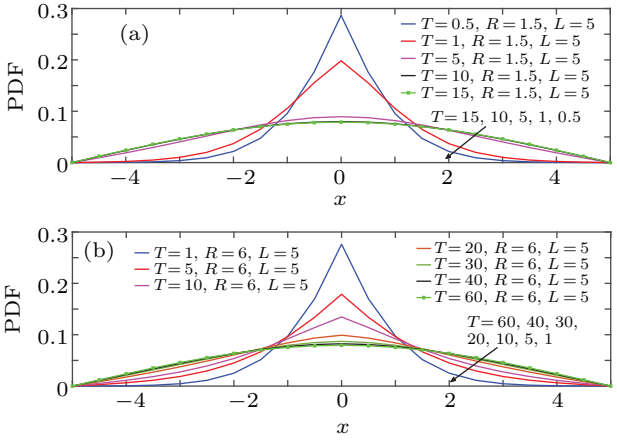


Fig. 3. Time evolution of PDF in the backbone of classical comb, along x direction, for $D = \tilde{D} = 1$, $L = 5$, and (a) $R = 1.5$, (b) $R = 6$.

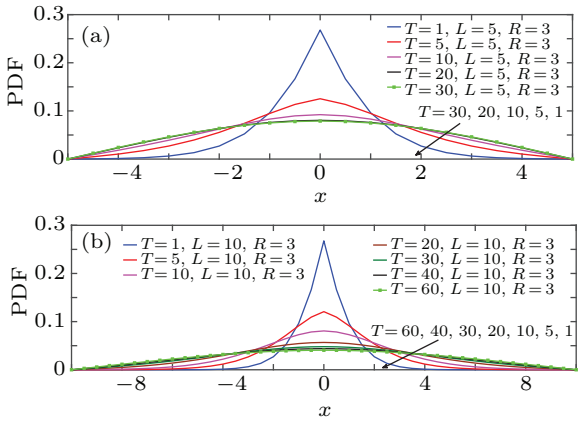


Fig. 4. Time evolution of PDF in the backbone of classical comb, along x direction, for $D = \tilde{D} = 1$, $R = 3$, and (a) $L = 5$, (b) $L = 10$.

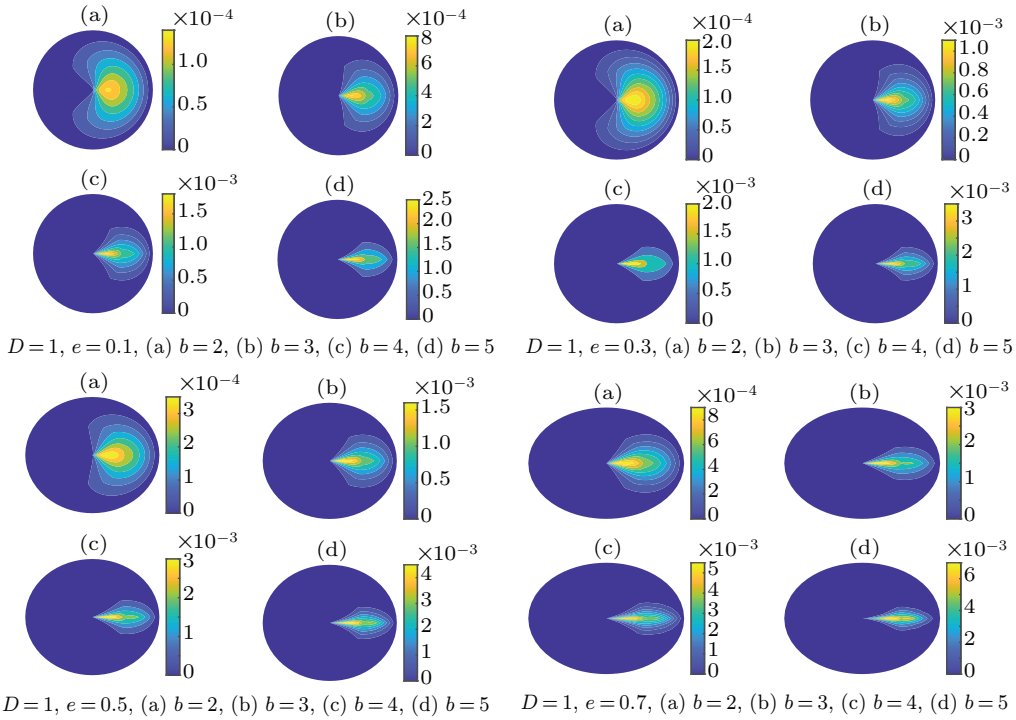


Fig. 5. Time evolution of probability distribution in the structure for different value of the parameter b at $T = 1$: (a) $D = \tilde{D} = 1$, $e = 0.5$, and $b = 2$, (b) $D = \tilde{D} = 1$, $e = 0.5$, and $b = 3$, (c) $D = \tilde{D} = 1$, $e = 0.5$, and $b = 4$, (d) $D = \tilde{D} = 1$, $e = 0.5$, and $b = 5$.

Figures 6 and 7 depict the temporal evolution of marginal PDF along θ direction when $R = 1/2$, which show a symmetrical and non-Gaussian behavior according to different parameters. Figure 6 shows that the diffusion process slows down as the length of lateral branches increases, which can be attributed to the elapsed time in radial dead ends until the particle returns to the backbone. Besides, as in classical comb, it converges to a non-Gaussian function after a period that varies according to the length of the finger b. However, unlike classical comb, this function also alters according to b. The effects of the eccentricity of elliptical channel e, for fixed b, on marginal PDF along θ direction are detailed in Fig. 7. It shows that the concentration at the initial position increases as the eccentricity increases. According to PDF quantity, the results can be summarized as following: The diffusion in a finite elliptical comb-like structure is abnormal and reaches a state of saturation after a period, which varies according to the stay time in lateral dead ends. Moreover, the concentration increases with the increase of the curvature of the elliptical channel, in which the increase of the curvature obstructs particle diffusion.

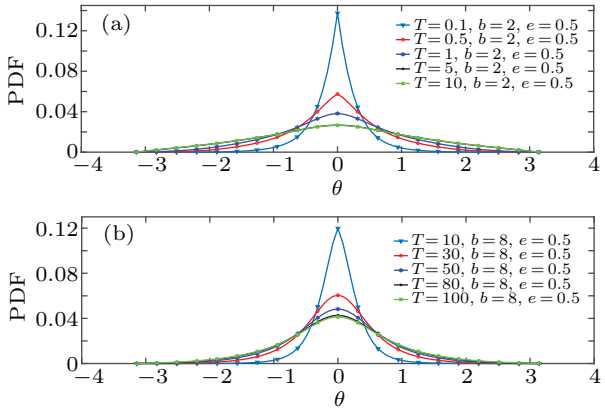


Fig. 6. Time evolution of PDF in the backbone of elliptical comb, along direction θ, for $D = \tilde{D} = 1$, $e = 0.5$, and (a) $b = 2$, (b) $b = 8$.

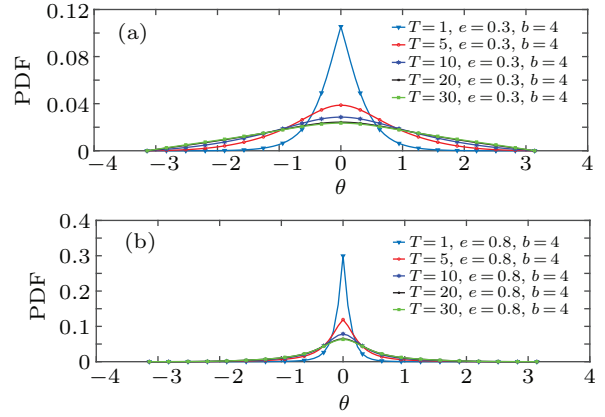


Fig. 7. Time evolution of PDF in the backbone of elliptical comb, along direction θ, for $D = \tilde{D} = 1$, $b = 4$, and (a) $e = 0.3$, (b) $e = 0.8$.

4.2. Mean square displacement

For more statistical information about this process and type of diffusion, the temporal evolution of the second moment (the mean square displacement (MSD) of the particle's positions), which describes the speed of particle motion, in the backbone is calculated as

$$\begin{aligned} \mathrm{MSD} &= \left\langle (x(t)-x_0)^2 \right\rangle \\ &= \int_{-\infty}^{\infty} (x(t)-x_0)^2 \mathrm{d}x \left(\int_{-\infty}^{\infty} P(x,y,t)\mathrm{d}y \right). \end{aligned} \tag{15}$$

Firstly, we revisit MSD along x direction in finite classical comb with respect to parameters R and L. We use numerical simulation to obtain $\left\langle (x(t)-x_0)^2 \right\rangle$, in which we assume $x_0 = 0$. As shown in Fig. 8, for fixed L, $\left\langle x^2(t) \right\rangle$ grows nonlinearly for a short time, then it converges to a fixed value. However, the speed of convergence decreases as R increases, which agrees with the results about PDF in the previous section. Besides, $\left\langle x^2(t) \right\rangle \sim t^{\alpha}$ with $\alpha < 1$ varies with respect to R and the transient sub-diffusion regimes dominate the process. Namely, one sub-diffusion regime will dominate the process as R tends to infinity. It should be noted that it has been established that $\left\langle x^2(t) \right\rangle \sim \sqrt{t}$ for infinite comb model. The effects of L on $\left\langle x^2(t) \right\rangle$ is represented in Fig. 9. It shows that the saturation threshold increases as L increases. Namely, the state of saturation will go away when L tends infinity. It should be mentioned that the saturation of the MSD is also found by considering diffusion in comb structures with stochastic resetting.[63,82]

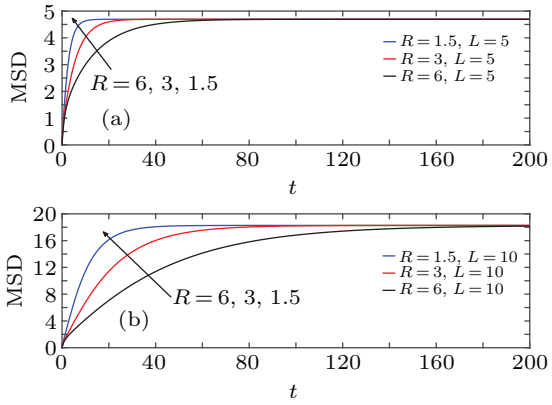


Fig. 8. Temporal evolution of MSD in the backbone of classical comb, along x direction for $D = \tilde{D} = 1$, $R = \{1.5, 3, 6\}$, and (a) $L = 5$, (b) $L = 10$.

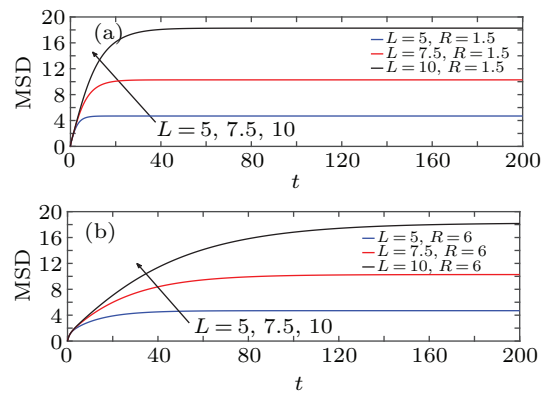


Fig. 9. Temporal evolution of MSD in the backbone of classical comb, along x direction for $D = \tilde{D} = 1$, $L = \{5, 7.5, 10\}$, and (a) $R = 1.5$, (b) $R = 6$.

Now, we consider the behavior of MSD along θ direction in elliptical comb. As in the case of diffusion in classical comb, Fig. 10 shows a non-linear behavior of MSD along θ direction, then it converges to constant value and the speed of convergence decreases as b increases. However, for fixed e, it does not converge to the same value, except in case of circle comb, i.e., when $e = 0$. Moreover, the saturating threshold is reduced as e increases. This can be attributed to increase the perimeter of the elliptical channel, $p \approx 2\pi\sqrt{(a^2+b^2)/2}$, and the time of stay in the fingers. For short time, Fig. 10 shows that MSD $\sim t^{\alpha}$ with $0 < \alpha < 1$, and a sub-diffusion process occurs in this direction. Besides, the value of exponent α decreases as e increases. Such transient sub-diffusion behavior was indeed demonstrated, for example, diffusion of fluorophore-labelled dextran (MW 3000) in granular layers (GL) of rat and turtle cerebella,[19] also diffusion in crowded media of non-inert obstacles.[83]

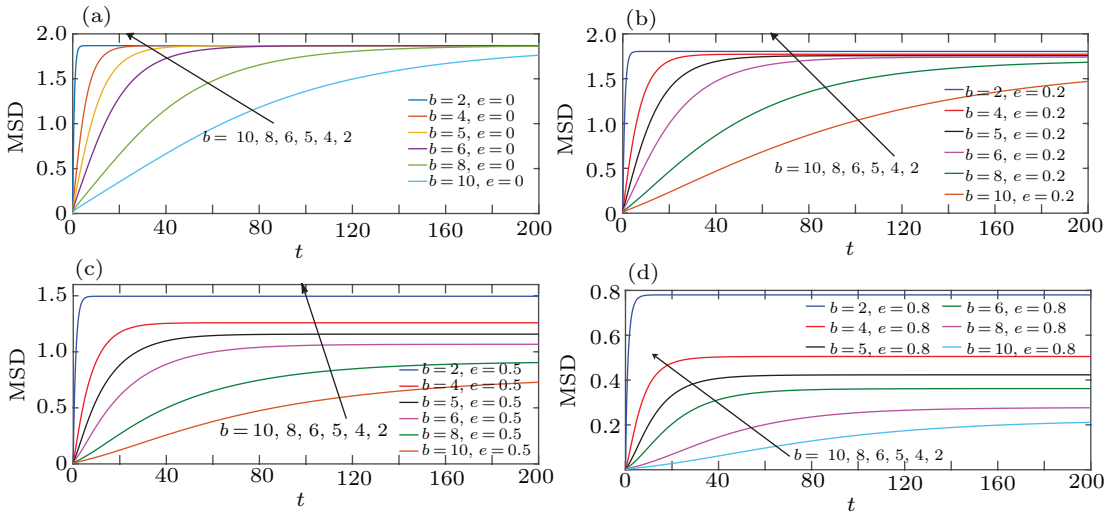


Fig. 10. Temporal evolution of MSD in the backbone of classical comb, along θ direction for $D = \tilde{D} = 1$, $b = \{2,4,5,6,8,10\}$, and (a) $e = 0$, (b) $e = 0.2$, (c) $e = 0.5$, (d) $e = 0.8$.

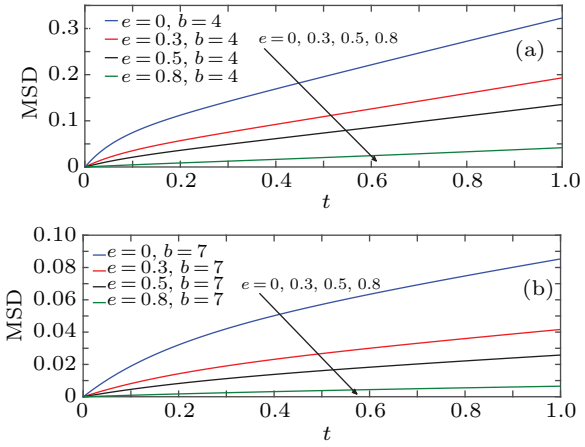


Fig. 11. MSD along θ direction for short time for $D = \tilde{D} = 1$, $e = \{0, 0.3, 0.5, 0.8\}$, and (a) $b = 4$, (b) $b = 7$.

4.3. Diffusion in the elliptical channel without dead ends

The phenomenon of slow diffusion can be attributed here to the time the particles spend in the dead ends until they return to the backbone and the obstruction due to curvature of the ellipse. For more about the role of eccentricity or curvature of the ellipse, we consider the diffusion in the structure with the absence of dead ends. MSD along the elliptical channel is plotted in Fig. 12. In contrast to diffusion in elliptical comb, MSD grows linearly with time, and the diffusion is normal, see Fig. 12(a). However, MSD grows non-linearly with time as the curvature of the channel increases, see Fig. 12(b), and sub-diffusion process is dominated.

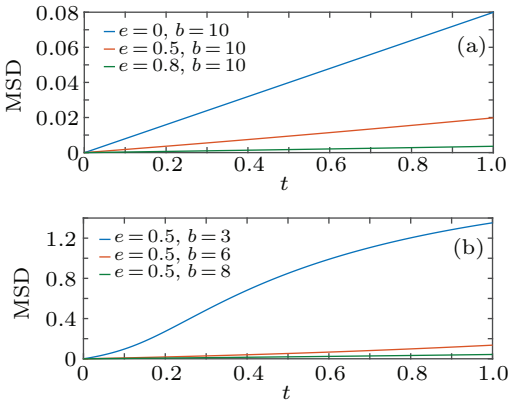


Fig. 12. MSD along elliptical channel without constrained geometries for short time for $D = \tilde{D} = 1$, and (a) $e = 0$, 0.5, 0.8, and $b = 10$, (b) $e = 0.5$ and $b = 3$, 6, 8.

5. Conclusion and perspectives

In this paper, we have considered the features of diffusion process in an elliptical channel with dead ends and discussed the impact of geometry of the structure on this process. To manipulate this problem, a modification of comb-like model has been suggested, in which the backbone and fingers of the comb correspond to the elliptical channel and radial dead ends distributed along it, respectively. The Fokker–Planck equation

that expresses the diffusion process in the structure process has been derived and solved numerically. The results show a transient sub-diffusion behavior dominates the process followed by a saturating state. The sub-diffusion regime and saturation threshold are affected by the length of the elliptical channel lateral branch and its curvature. Besides, the concentration of particles at the initial position increases with the increase in the curvature of the elliptical channel. These established results can be added to the results of previous works that refer to the effects of curvature on diffusion processes in curved channels.

Acknowledgement

Project supported by the National Natural Science Foundation of China (Grant Nos. 11772046 and 81870345).

References

[1] Stein W D 1986 *Transport and diffusion across cell membranes* (Academic Press)
[2] Bressloff P C 2014 *Stochastic Processes in Cell Biology* (Springer)
[3] Sibatov R T and Uchaikin V V 2015 *J. Comput. Phys.* **293** 409
[4] Mendez V, Fedotov S and Horsthemke W 2010 *Reaction-Transport Systems* (Springer)
[5] Viswanathan G M, Luz M, Raposo E P and Stanley H E 2011 *The Physics of Foraging* (Cambridge University Press)
[6] Dix J A and Verkman A S 2008 *Annu. Rev. Biophys.* **37** 247
[7] Weiss M, Hashimoto H and Nilsson T 2003 *Biophys. J.* **84** 4043
[8] Höfling F and Franosch T 2013 *Rep. Prog. Phys.* **76** 46602
[9] Sun H G, Sheng H, Chen Y Q, Chen W and Yu Z B 2013 *Chin. Phys. Lett.* **30** 46601
[10] Wu W X, Zheng Z G, Song Y L, Han Y R, Sun Z C and Li C P 2020 *Chin. Phys. B* **29** 90503
[11] Wang B, Kuo J, Bae S C and Granick S 2015 *Nat. Mater.* **11** 481
[12] Metzler R, Jeon J H and Cherstvy A G 2016 *Biochim. Biophys. Acta - Biomembr.* **1858** 2451
[13] Metzler R 2020 *Eur. Phys. J. Spec. Top.* **229** 711
[14] Metzler R 2017 *Biophys. J.* **112** 413
[15] Jeon J H, Javanainen M, Martinez-Seara H, Metzler R and Vattulainen I 2016 *Phys. Rev. X* **6** 21006
[16] Szymanski J and Weiss M 2009 *Phys. Rev. Lett.* **103** 38102
[17] Gupta S, Mel J, Perera R M, Zolnierczuk P and Schneider G J 2018 *J. Phys. Chem. Lett.* **9** 2956
[18] Tabei S, Burov S, Kim H Y, Kuznetsov A, Huynh T, Jureller J, Philipson L H, Dinner A R and Scherer N F 2013 *Proc. Natl. Acad. Sci. USA* **110** 4911
[19] Xiao F, Hrabe J and Hrabetova S 2015 *Biophys. J.* **108** 2384
[20] Goeppert N, Goldscheider N and Berkowitz B 2020 *Water Res.* **178** 115755
[21] Caspi A, Granek R and Elbaum M 2000 *Phys. Rev. Lett.* **85** 5655
[22] Reverey J F, Jeon J H, Bao H, Leippe M, Metzler R and Selhuber-Unkel C 2015 *Sci. Rep.* **5** 11690
[23] Rammal R and Toulouse G 1983 *J. Phys. Lett.* **44** 13
[24] Sokolov I M 2012 *Soft Matter* **8** 9043
[25] Metzler R, Jeon J H, Cherstvy A G and Barkai E 2014 *Phys. Chem. Chem. Phys.* **16** 24128
[26] Ben-Avraham D and Havlin S 2000 *Diffusion and reactions in fractals and disordered systems* (Cambridge university press)
[27] Gao S L, Zhong S C, Wei K and Ma H 2012 *Acta Phys. Sin.* **61** 6 (in Chinese)
[28] Goodknight R C, Klikoff W A and Fatt I 1960 *J. Phys. Chem.* **64** 1162
[29] Pinner A and Nye P H 1982 *J. Soil Sci.* **33** 25
[30] Rao P, Jessup R E and Addiscott T M 1982 *Soil Sci.* **133** 154
[31] Tao A, Tao L and Nicholson C 2005 *J. Theor. Biol.* **234** 525
[32] Hrabe J, HrabeTová S and Segeth K 2004 *Biophys. J.* **87** 1606
[33] Ernest P and S. B R 1964 *J. Gen. Physiol.* **47** 1129
[34] Safford R E, Bassingthwaighte E A and Bassingthwaighte J B 1978 *J. Gen. Physiol.* **72** 513
[35] Santamaria F, Wils S, De Schutter E and Augustine G J 2006 *Neuron* **52** 635
[36] Iomin A, Mendéz V and Horsthemke W 2018 *Fractional dynamics in comb-like structures* (World Scientific)
[37] Weiss G H and Havlin S 1986 *Phys. A* **134** 474
[38] Weiss G H and Havlin S 1987 *Philos. Mag. B* **56** 941
[39] Arkhincheev V E and Baskin E M 1991 *Sov. Phys. JETP* **73** 161
[40] Méndez V, Iomin A, Horsthemke W and Campos D 2017 *J. Stat. Mech. Theory Exp.* **2017**
[41] Méndez V and Iomin A 2013 *Chaos Soliton. Fract.* **53** 46
[42] Iomin A 2012 *Phys. Rev. E* **86** 32101
[43] Arkhincheev V E, Kunnen E and Baklanov M R 2011 *Microelectron. Eng.* **88** 694
[44] Liu L 2018 *J. Comput. Math.* **36** 563
[45] Liu L, Zheng L and Liu F 2017 *J. Mol. Liq.* **233** 326
[46] Iomin A and Méndez V 2016 *Chaos Soliton. Fract.* **82** 142
[47] Dzhanoev A R and Sokolov I M 2018 *Chaos Soliton. Fract.* **106** 330
[48] Havlin S, Kiefer J E and Weiss G H 1987 *Phys. Rev. A* **36** 1403
[49] Yuste S B, Abad E and Baumgaertner A 2016 *Phys. Rev. E* **94** 012118
[50] Iomin A 2011 *Phys. Rev. E* **83** 052106
[51] Sandev T, Iomin A and Kantz H 2015 *Phys. Rev. E* **91** 032108
[52] Sandev T, Iomin A and Kantz H 2017 *Phys. Rev. E* **95** 52107
[53] Fan Y, Liu L, Zheng L and Li X 2019 *Sci. Numer. Simul.* **77** 225
[54] Wang Z and Zheng L 2020 *Phys. A* **549** 123889
[55] Iomin A 2021 *Chaos Soliton. Fract.* **142** 110488
[56] Suleiman K, Zheng L, Liu C, Zhang X and Wang E 2020 *Int. Commun. Heat Mass Transf.* **117** 104733
[57] Suleiman K, Song Q, Zhang X, Liu S and Zheng L 2022 *Chaos Soliton. Fract.* **155** 111742
[58] Saxton M J 2007 *Biophys. J.* **92** 1178
[59] Baskin E and Iomin A 2004 *Phys. Rev. Lett.* **93** 120603
[60] Sandev T, Iomin A and Kocarev L 2020 *Phys. Rev. E* **102** 042109
[61] Singh R K, Sandev T, Iomin A and Metzler R 2021 *J. Phys. A* **54** 404006
[62] Wang Z, Lin P and Wang E 2021 *Chaos Soliton. Fract.* **148** 111009
[63] Sandev T, Domazetoski V, Iomin A and Kocarev L 2021 *Mathematics* **9** 1
[64] Dagdug L, Berezhkovskii A M, Makhnovskii Y A and Zitserman V Y 2007 *J. Chem. Phys.* **127** 224712
[65] Berezhkovskii A M and Dagdug L 2011 *J. Chem. Phys.* **134** 124109
[66] Ogawa N 2010 *Phys. Rev. E* **81** 61113
[67] Ogawa N 2013 *Phys. Lett. A* **377** 2465
[68] Chávez Y, Chacón-Acosta G and Dagdug L 2018 *J. Chem. Phys.* **148** 214106
[69] Castro-Villarreal P, Villada-Balbuena A, Méndez-Alcaraz J M, Castañeda-Priego R and Estrada-Jiménez S 2014 *J. Chem. Phys.* **140** 214115
[70] Assenza S and Mezzenga R 2018 *J. Chem. Phys.* **148** 54902
[71] Dobrowolski T and Jarmoliński A 2018 *Results Phys.* **8** 48
[72] Burada P S, Hnggi P, Marchesoni F, Schmid G and Talkner P 2010 *Chem. Phys. Chem.* **10**
[73] Bénichou O, Illien P, Oshanin G, Sarracino A and Voituriez R 2018 *J. Phys. Condens. Matter* **30** 443001
[74] Hrabětová S, Hrabe J and Nicholson C 2003 *J. Neurosci.* **23** 8351
[75] Nicholson C and Hrabětová S 2017 *Biophys. J.* **113** 2133
[76] Tao L and Nicholson C 2004 *J. Theor. Biol.* **229** 59
[77] Sykova E and Nicholson C 2008 *Physiol. Rev.* **88** 1277
[78] Bueno-Orovio A, Kay D, Grau V, Rodriguez B and Burrage K 2014 *J. R. Soc. Interface* **11** 20140352
[79] Wolak D J and Thorne R G 2013 *Mol. Pharm.* **10** 1492
[80] Vendel E, Rottschfer V and Lange E 2019 *Fluids Barriers CNS* **16** 12
[81] Caratelli D, Natalini P, Ricci P E and Yarovoy A 2010 *Appl. Math. Comput.* **216** 556
[82] Domazetoski V, Masó-Puigdellosas A, Sandev T, Méndez V, Iomin A and Kocarev L 2020 *Phys. Rev. Res.* **2** 033027
[83] Ghosh S K, Cherstvy A G and Metzler R 2014 *Phys. Chem. Chem. Phys.* **17** 1847